

Aerodynamic Design and Blade Angle Analysis of a Small Horizontal–Axis Wind Turbine

Mohamed Khaled¹, Mostafa Mohamed Ibrahim², Hesham ElSayed Abdel Hamed²,
Ahmed Farouk Abdel Gawad³

¹Demonstrator in the Higher Institute of Engineering at El Sherouk City, Cairo, Egypt

²Mechanical Power Engineering Department, Faculty of Engineering, Zagazig University, Zagazig, Egypt

³Faculty of Engineering, Zagazig University, Zagazig, Egypt

Email address:

dr_mostafa48@yahoo.com (M. M. Ibrahim)

To cite this article:

Mohamed Khaled, Mostafa Mohamed Ibrahim, Hesham ElSayed Abdel Hamed, Ahmed Farouk Abdel Gawad. Aerodynamic Design and Blade Angle Analysis of a Small Horizontal–Axis Wind Turbine. *American Journal of Modern Energy*. Vol. 3, No. 2, 2017, pp. 23-37. doi: 10.11648/j.ajme.20170302.12

Received: May 9, 2017; **Accepted:** May 25, 2017; **Published:** June 30, 2017

Abstract: The wind turbine blades are the main part of the rotor. Extraction of energy from wind depends on the design of the blade. In this paper, a design method based on Blade Element Momentum (BEM) theory is explained for small horizontal–axis wind turbine model (HAWT) blades. The method was used to optimize the chord and twist distributions of the wind turbine blades to enhance the aerodynamic performance of the wind turbine and consequently, increasing the generated power. A Fortran program was developed to use (BEM) in designing a model of Horizontal–Axis Wind Turbine (HAWT). NACA 4412 airfoil was selected for the design of the wind turbine blade. Computational fluid dynamics (CFD) analysis of HAWT blade cross section was carried out at various blade angles with the help of ANSYS Fluent. Present results are compared with other published results. Power generated from wind turbine increases with increasing blade angle due to the increase in air–velocity impact on the wind turbine blade. For blade angle change from 20° to 60°, the turbine power from wind has a small change and reaches the maximum when the blade angle equals to 90°. Thus, HAWT power depends on the blade profile and its orientation.

Keywords: Renewable Energy, HAWT Design, Blade Element Momentum Theory, Airfoil Aerodynamic, Blade Angle

1. Introduction

A wind turbine is a generic term for machines with rotating blades that convert the kinetic energy of wind into useful power. The basic idea has been around for a long time but modern wind turbines are a far from the original designs. Modern turbines evolved from the early designs and are typically classified as one or more blades. Most of the turbines used today have three blades. The rotational speed is a very important design factor. Turbines operating at a constant rotor speed have been fomenting up to now, but turbines with variable rotational speed are becoming increasingly more common with the desire to optimize the captured energy, lower stress, and obtain better power quality. There are many different wind turbine classes, but two stands out as the best known: the vertical–axis turbine (VAWT), and the horizontal–axis turbine (HAWT) [1].

The objectives of this study are: (i) using BEM theory for aerodynamic design of the HAWT blades and performance analysis of the existing blades, (ii) building a computer program using this method to design a small HAWT rotor, (iii) studying the effect of blade angle on the turbine output power.

2. Literature Review

Kulunk and Yilmaz [11] explained a design method based on blade element momentum (BEM) theory for horizontal–axis wind turbine (HAWT) blades. The method was used to optimize the chord and twist distributions of the blades. They applied their method to generate a 100kW HAWT rotor. Their computer program estimated the aerodynamic performance of some existing HAWT blades.

Tenguria et al. [16] designed a horizontal–axis wind turbine blade with the help of Glauert's optimal rotor theory

and developed a computer program for getting the chord, thickness and twist distributions while maintaining the lift coefficient constant throughout the blade. The wind turbine blade was divided into 19 sections and each section had the same length. Blade is modeled with ANSYS with airfoil NACA 634–221. First analysis of the blade was done with the spar of square shape and for validation their results were compared with experimental work. A new shape of spar of combined shape (box and cross) was used for a second analysis and the results showed that the deflection of cap and web reduces at both root and transition segment.

Chandrala et al. [3] carried out a study concerning the aerodynamic efficiency of wind turbine blade when tested in wind tunnel. They selected NACA 4420 airfoil for analysis. CFD Analysis of HAWT blade was carried out at various blade angles with help of ANSYS CFX. Their computational results were compared with experimental results. They stated that HAWT efficiency is highly-dependent on the blade profile and its orientation.

Kale and Sapali [10] determined the blade parameters, such as chord and thickness distributions along the blade for one mega-watt (MW) wind turbine on the basis of strength and aerodynamics. The blade geometry was based on the modified NACA 63-621 and FX 66S-196 series profiles. The cylindrical profile was selected near the blade root for easy connection with rotor hub and to assure the structural strength on the inner part of blade.

Chaudhary and Roy [4] presented the design and optimization of the rotor blade performance for a 400W small wind turbine at the lower values of operating wind speed based on blade element momentum theory (BEM). The main focus was on the relationship between solidity, pitch angle, tip speed ratio, and maximum power coefficient. In their study, airfoil SG 6043 was selected. Their studies were conducted for variable chord and twisted blade with solidities in the range of 2% to 30% and blade numbers 3, 5, 7, 12, and 15 with rotor diameter of 2 m. These values of blade geometry parameters that were generated in MATLAB were exported to Q-Blade software. To give results in terms of power coefficient curve ($C_p - \lambda$). Hence, maximum power coefficient was obtained for the solidity in the range of 3% to 12% for a number of blades of 3, 5, and 7.

Kumar et al. [12] changed the wind turbine blade material from epoxy glass to epoxy carbon to improve the wind turbine performance. The modeling and the static and dynamic structural analysis was carried out by using ANSYS software. The static analysis results indicated that epoxy carbon material undergoes the minimum deformation of 729 mm as compared to the other material epoxy glass. The Minimum Von-misses stress of 0.035 MPa was observed in epoxy carbon material as compared to the other material. From strength and stiffness point of view, epoxy carbon materials performing better than the other material considered in their work.

Hu et al. [9] studied numerically the feasibility of improving blade power by applying vortex generators to large variable propeller shaft horizontal-axis wind turbines

(2 MW). Three different chordwise installation positions of vortex generators were designed according to transition and separation lines at the blade root. Calculation results showed that the blade aerodynamic power increased by 0.6%. It can be seen from the vorticity contours in the different downstream spanwise position of vortex generators that it is not appropriate to install vortex generators with the same size in different positions of blades. Their results indicated that it is feasible to improve aerodynamic power by applying vortex generators to large variable propeller shaft wind turbines.

Mostafa et al. [15] studied the dynamic behavior of aerodynamic, mechanical and electrical parts of customized variable-speed variable-pitch wind turbine equipped with a permanent magnet synchronous generator. They investigated Aeolos 50 kw wind turbine, drive train, and permanent magnet synchronous generator using simulating program Matlab/simulink. Two controllers for blade pitch angle and torque generator were investigated to guarantee the output power almost constant. Their strategy appeared better than classical approaches according to rotor speed and output power.

Derakhshan and Tavaziani [5] investigated aerodynamic performance of wind turbines. Flow around wind turbine was simulated with Navier-Stokes equations using three difference turbulence models (Spalart–Allmaras, $K - \epsilon$ and SST $K - \omega$) and results were compared with experimental data. According to numerical results, at 5 m/s to 10 m/s wind speeds (low speeds), the three turbulence models had similar predictions in power. But at higher wind speeds, $K - \epsilon$ predicted with more accuracy, thus, $K - \epsilon$ is the best between the three models. Based on their results, they suggested $K - \epsilon$ Launder Sharma turbulence model using Hakimi precondition for the prediction of performance of horizontal-axis wind turbines.

Based on the above literature survey, it is clear that there is a need for showing the effect of blade angle of another airfoil profile, increasing the range of blade angles between 0° and 90°, and illustrating the distributions of pressure coefficient and vorticity around airfoil profile.

3. Blade Design Procedure

This section describes the calculation method for wind turbine blades, which can be used to design the wind turbine blade using BEM theory.

BEM theory equates two methods of examining how a wind turbine operates. The first method is to use a momentum balance on a rotating annular stream tube passing through a turbine. The second is to examine the forces generated by the aerofoil lift and drag coefficients at various sections along the blade. Figure (1) shows the overall flow situation, relationship of the various angles and velocities at the wind turbine blade [17].

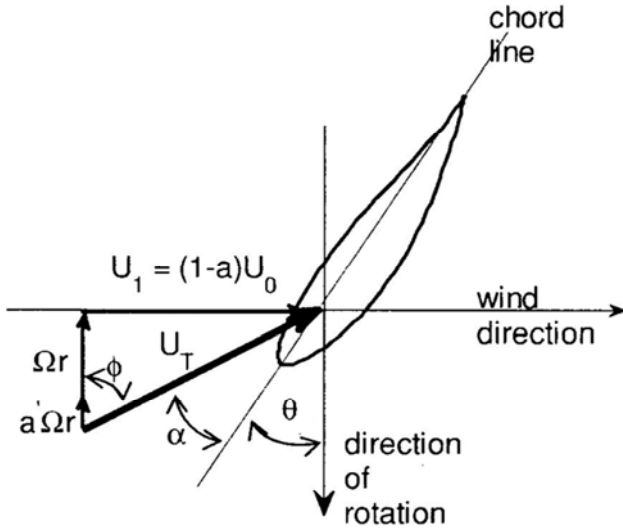


Figure 1. Velocities for blade element at radius r [17].

These two methods give a series of equations that can be solved iteratively. Blade element theory relies on two key assumptions:

- There are no aerodynamic interactions between different blade elements.
- The forces on the blade elements are solely determined by the lift and drag coefficients.

Consider a blade with N division elements as shown in figure (2), each one of the blade elements experiences a slightly different flow as they have a different rotational speed (Ωr), a different chord length (C) and a different twist angle (θ).

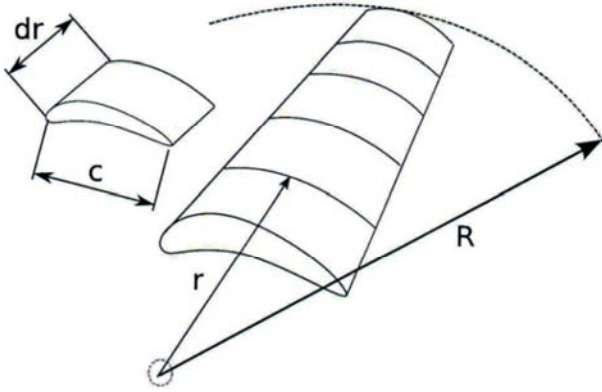


Figure 2. The Blade Element Model [14].

Blade element theory involves dividing up the blade into a sufficient number of elements and calculating the flow at each one. Overall performance characteristics are determined by numerical integration along the blade span. In practice, the flow is slightly turned as it passes over the airfoil. Thus, in order to obtain a more accurate estimate of airfoil performance; the average flow conditions at inlet and exit are used to estimate performance. Then, obtain and examine the empirical curves for the aerodynamic properties of the airfoil at each section (the airfoil may vary from the root to the tip), i.e., C_L vs. α , C_D vs. α . Choose the design aerodynamic

conditions, $C_{L, design}$ and α_{design} , such that $(C_L/C_D)_{design}$ is at a maximum value for each blade section using Q-blade software[13].

The flow around the wind turbine blades starts. At inlet to the blade, the flow is not rotating. At exit from the blade row, the flow rotates at rotational speed ω . That is, over the blade row wake rotation has been introduced. The average rotational flow over the blade due to wake rotation is therefore $(\omega/2)$. The blade is rotating with speed (Ω). The average tangential velocity (that the blade experiences) is therefore $\left(\Omega r + \frac{\omega r}{2}\right)$. [7]

Because the pressure on the suction side of a blade is lower than that on the pressure side, air tends to flow around the tip from the lower to upper surface, reducing lift and hence power production near the tip. This effect is most noticeable with fewer, wider blades. A number of methods have been suggested for including the effect of the tip loss. The most straight forward approach to use is one developed by Prandtl [1]. According to this method, a correction factor, F , must be introduced into the previously discussed equations. This correction factor is a function of the number of blades, the angle of relative wind, and the position on the blade. Based on Prandtl's method:

$$F = \left(\frac{2}{\pi}\right) \cos^{-1} \left[\exp \left(- \left\{ \frac{(B/2) [1 - (r/R)]}{(r/R) \sin \phi} \right\} \right) \right] \quad (1)$$

F is always between 0 and 1. This tip loss correction factor characterizes the reduction in the forces at a radius (r) along the blade that is due to the tip loss at the end of the blade.

The tip loss correction factor affects the forces derived from momentum theory. Thus, equations become: [1]

$$dQ = 4\pi F \rho U \Omega a' (1-a) r^3 dr \quad (2)$$

$$dT = 4F\pi\rho U^2 a (1-a) \pi r dr \quad (3)$$

$$a'/(1-a) = \sigma C_L / 4F \lambda_r \sin \phi \quad (4)$$

$$a/(1-a) = \sigma C_L \cos \phi / 4F \sin^2 \phi \quad (5)$$

$$C_L = \frac{4F \sin \phi (\cos \phi - \lambda_r \sin \phi)}{\sigma (\sin \phi + \lambda_r \cos \phi)} \quad (6)$$

$$a = \frac{1}{1 + \frac{4F \sin^2 \phi}{\sigma C_L \cos \phi}} \quad (7)$$

$$a' = \frac{1}{1 + \frac{4F \cos \phi}{\sigma C_L - 1}} \quad (8)$$

$$C_P = \frac{8}{\lambda_r^2} \int_{\lambda_{r,n}}^{\lambda} F \lambda_r^3 a^3 (1-a) \left(1 - \frac{C_D}{C_L} \cot \theta\right) d\lambda_r \quad (9)$$

The aerodynamic design of optimum rotor blades from a known airfoil type means determination of the geometric parameters such as chord length distribution and twist distribution along the blade length for a certain tip-speed ratio at which maximum power coefficient of the rotor exists. For this reason, the change of the power coefficient of the rotor with respect to tip-speed ratio should be figured out in order to determine the design tip speed ratio, λ_d , corresponding to which the rotor has a maximum power coefficient. The blade design parameters will then be according to this tip speed ratio. [8]

A general relationship can be obtained between optimum relative wind angle and local tip-speed ratio which will be applicable for any airfoil type [1]

$$\frac{\partial}{\partial \varphi} [\sin^2 \varphi (\cos \varphi - \lambda_r \sin \varphi) (\sin \varphi + \lambda_r \cos \varphi)] = 0 \quad (10)$$

Equation (10) reveals after some algebra [1]

$$\varphi_i = \frac{2}{3} \tan^{-1} \left(\frac{1}{\lambda_{r,i}} \right) \quad (11)$$

Having found the solution of determining the optimum relative wind angle for a certain local tip-speed ratio, the rest is nothing but to apply the equations from Eq. (6) to (9), which were derived from the blade-element momentum theory and modified including the tip loss factor, to define the blade shape and to find out the maximum power coefficient for a selected airfoil type. Dividing the blade length into N elements, the local tip speed ratio for each blade element can then be calculated as:

$$\lambda_{r,i} = \lambda \frac{r_i}{R} \quad (12)$$

Also, the tip loss correction factor for each element can be calculated as:

$$F = \left(\frac{2}{\pi} \right) \cos^{-1} \left[\exp \left(- \left\{ \frac{(B/2) [1 - (r/R)]}{(r/R) \sin \varphi} \right\} \right) \right] \quad (13)$$

Chord-length distribution can then be calculated for each blade element by using the equation (14)

$$C_i = \frac{8\pi r_i F_i \sin \varphi_i (\cos \varphi_i - \lambda_{r,i} \sin \varphi_i)}{B C_{L,design} (\sin \varphi_i + \lambda_{r,i} \cos \varphi_i)} \quad (14)$$

Where $C_{L,design}$ is chosen such that the glide ratio is minimum at each blade element. The twist distribution can easily be determined by using equation (15).

$$\theta_i = \varphi_i - \alpha_{i,design} \quad (15)$$

Where α_{design} is again the design angle of attack at which $C_{L,design}$ is obtained.

Now, the parameters such as chord-length and twist distribution along the blade length are known and in this case lift coefficient and angle of attack have to be determined from the known blade geometry parameters.

This requires an iterative solution in which for each blade element the axial and angular induction factors are firstly taken as the values which were found for the corresponding designed blade elements and then determined within an acceptable tolerance of the previous guesses of induction factors during iteration. Applying the design procedure explained, a Fortran program was written to design wind turbine blade for two different types of airfoils.

4. Analytical Model

The first step of wind blade design is to select the airfoil profile and obtain its design parameters. Figure (3) shows the NACA 4412 airfoil which is selected as an airfoil profile for a small wind turbine. [13]

Lift and drag coefficients for NACA 4412 aerofoil are shown in Figure (4) and the ratio of lift coefficient to drag coefficient (C_L/C_D) is shown in Figure (5). This plot obtained from Q-blade program which shows that for low values of angle of attack the aerofoil successfully produces a large amount of lift with little drag. At around $\alpha = 15^\circ$ a phenomenon known as stall occurs where there is a massive increase in drag and a sharp reduction in lift.

The design point must be selected to achieve maximum lift coefficient and minimum drag coefficient [6]. So, select the design point at maximum ratio of lift coefficient to drag coefficient $(C_L/C_D)_{maximum}$. From Figure (3), choose the design point for NACA 4412 airfoil as shown in table (1).

Table 1. Design Parameters for NACA 4412 airfoil.

Parameter	Design Value
Angle of attack	$\alpha_{design} = 5.85^\circ$
Lift coefficient	$C_{L,design} = 1.1106$
Drag coefficient	$C_{D,design} = 0.00828$
Ratio between lift and drag coefficient	$(C_L/C_D)_{design} = 134.13$

In the previous section, the design of a HAWT blade was explained and the solution method has been shown via the derived equations from BEM theory for NACA 4412 airfoil blade. The method of determining blade shape for optimum performance of a turbine was developed. The geometry and configuration of the designed rotor is summarized. Table (2) shows that the rotor uses NACA 4412 airfoil profile at inboard, mid-span and outboard stations of the blades. The NACA 4412 profile is also uniquely defined by its coordinates.

Table 2. Design blade for NACA 4412 airfoil.

Parameter	Value	Parameter	Value
Hub radius	0.035 m	Maximum chord	0.068710 m
Tip radius	0.35 m	Maximum chord station	0.073293 m
Blade length	0.315 m	Number of blades	3
Airfoil profile	NACA 4412	Designed wind speed	6 m/s
Mid-span airfoil	NACA 4412	Output power	27 W
Tip airfoil	NACA 4412	Tip speed ratio	5

Figures (6) – (8) show the blade geometry at the wind speed of 6 m/s and the output power of 27W. Figure (6) shows the change of the airfoil chord length relative to the rotor tip radius from blade hub to blade tip. It is clear that the airfoil chord length is decreased from hub radius (hub chord=0.068710 m) to tip radius (tip chord=0.003 m).

Figure (7) shows the change of relative wind angle through the blade length. The relative wind angle changes from hub radius (42.29°) to tip radius (7.61°). Figure (8) shows the change of blade twist angle of blade through the blade length. The blade twist angle changes from hub radius (36.44°) to tip radius (1.72°).

Figure (9) shows both axial and radial induction factors along the blade length. Axial induction factor has a small increase from (0.298346) at blade hub to (0.332332) at blade tip. Angular induction factor decreases from (0.542757) at blade hub to (0.009121) at blade tip.

Figure (10) shows tip losses correction factor along the blade length. Tip losses correction factor is almost constant (its value equal unity) along the blade from hub to 80% of blade height. But near blade tip, it decreases from (0.919721) at 80% to (0.394651) at blade tip.

Figure (11) shows local thrust coefficient along the blade length. local thrust coefficient is almost constant (its value equal 0.8) along the blade from hub to 80% of blade height. But near blade tip, it decreases from (0.8) at 80% to (0.350624) at blade tip.

Figure (12) shows solidity ratio along the blade length. It is clear that the solidity ratio is decreased from (0.937335) at blade hub to (0.012732) at blade tip.

Figure (13) shows power coefficient with tip speed ratio. The power coefficient is increased with increase of the tip speed ratio till it reaches the maximum value (0.536671) at tip speed ratio (5), then power coefficient decreases with increase of the tip speed ratio.

Figure (14) shows three views for three-dimensional wind turbine blade profile.

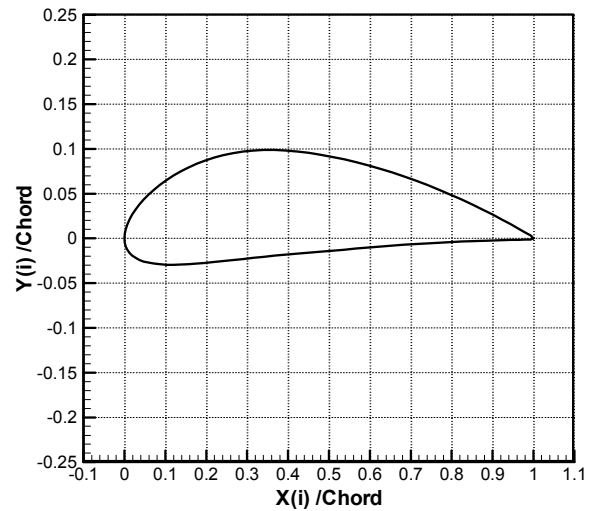
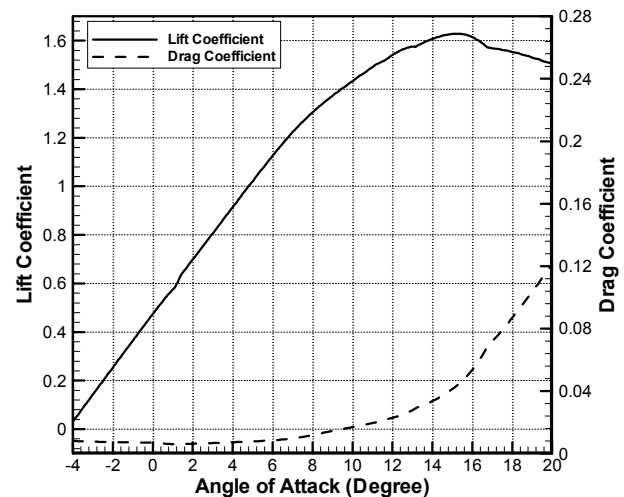
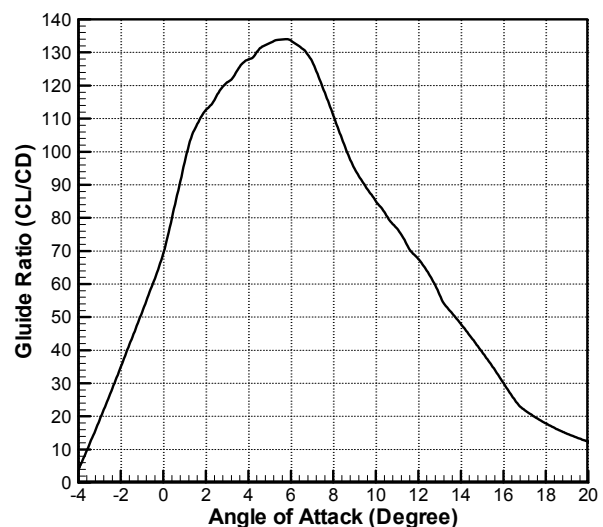
5. Effect of Blade Setting Angle (Computational Investigation)

5.1. Geometry and Grid Generation

Aerofoil NACA 4412 was modeled with chord length equal unity. Structured grids (C – type) were used in airfoil modeling for comparing of the accuracy of the simulation results.

To allow the air flow to be fully expanded, the length of computational domain using structured grid was determined

at 32.5 times that of the chord length, and the width was determined at 25 times that of the chord length as shown in Figure (15). [2]

**Figure 3.** NACA 4412 airfoil profile.**Figure 4.** Lift and drag coefficients.**Figure 5.** Ratio of lift coefficient to drag coefficient.

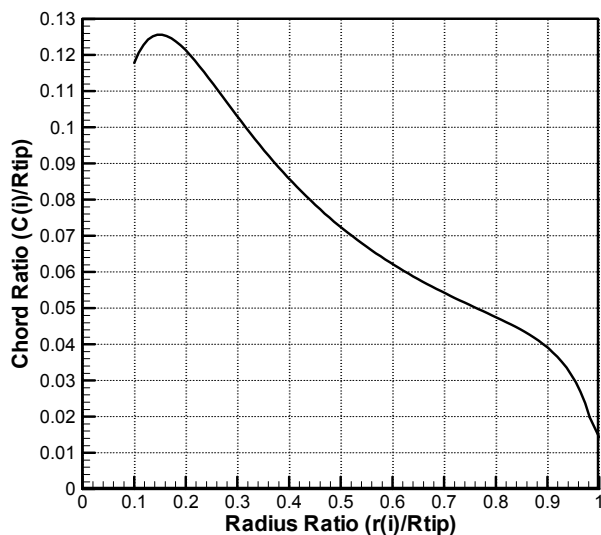


Figure 6. Airfoil chord distribution along the blade length.

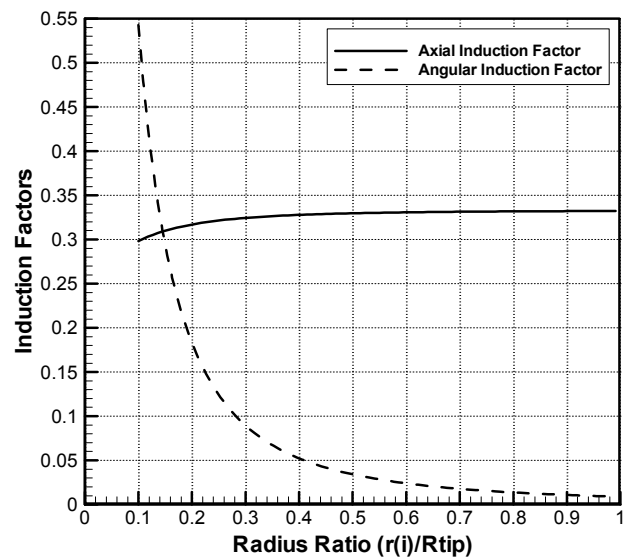


Figure 9. Induction factors along the blade length.

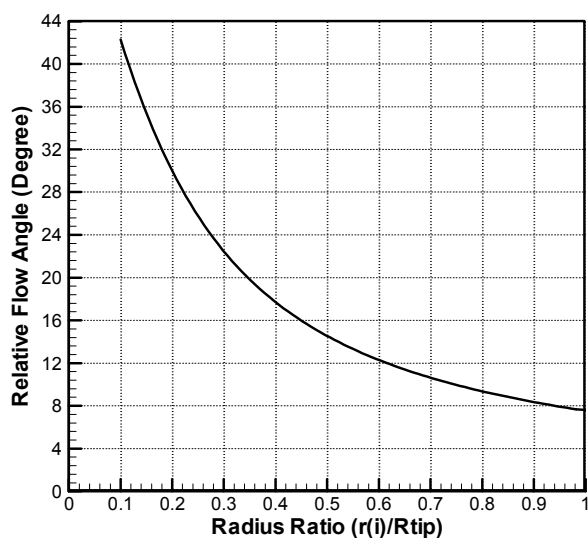


Figure 7. Airfoil relative wind angle along the blade length.

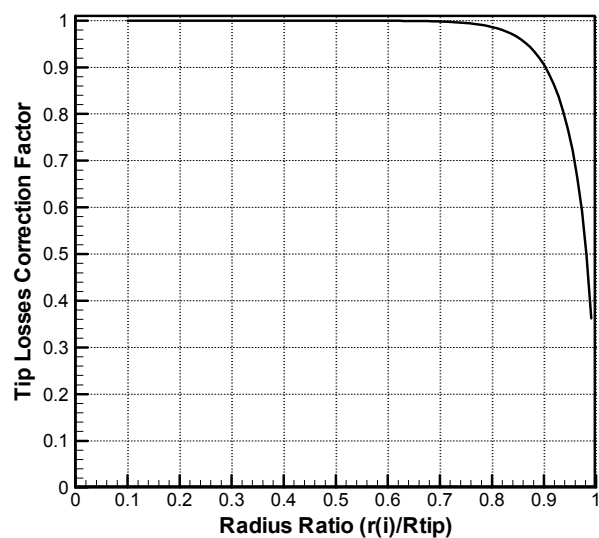


Figure 10. Tip losses correction factor along the blade length.

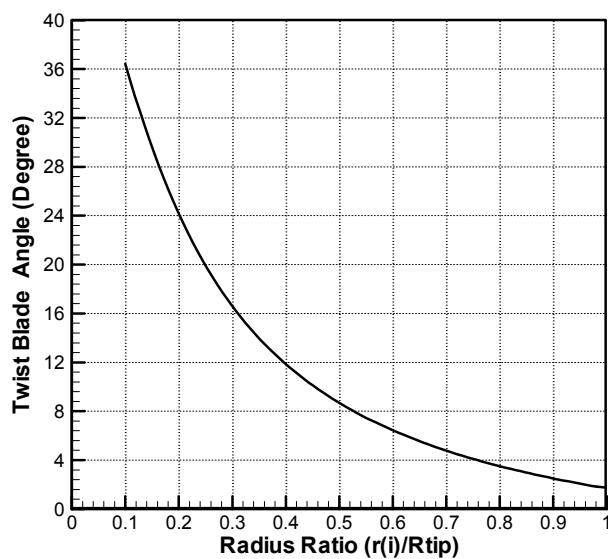


Figure 8. Airfoil twist angle along the blade length.

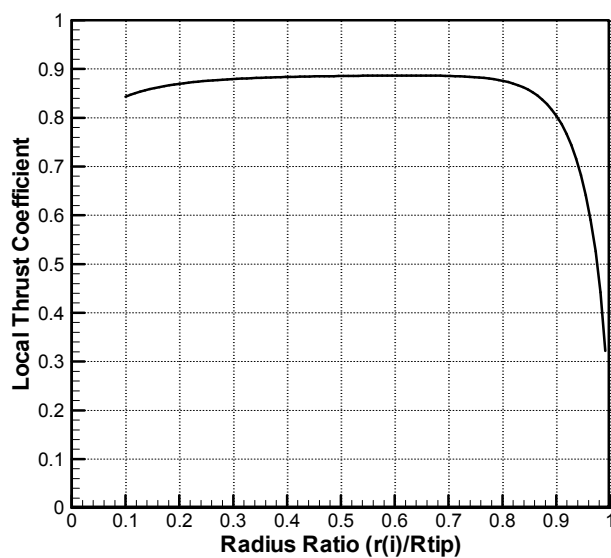


Figure 11. Local thrust coefficient along the blade length.

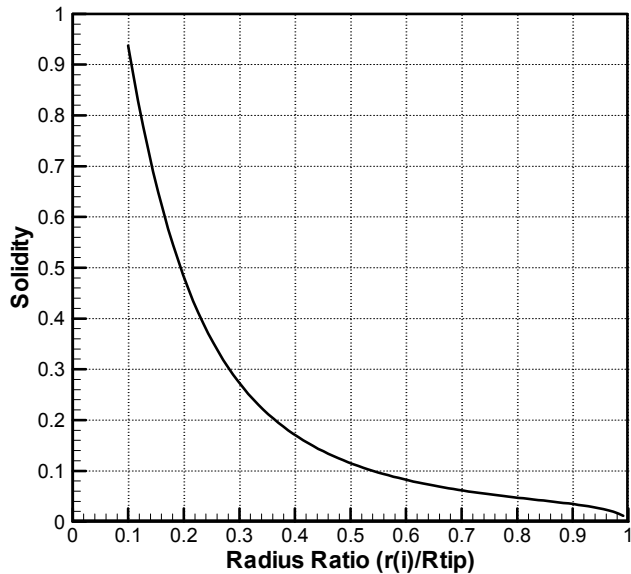


Figure 12. Solidity ratio along the blade length.

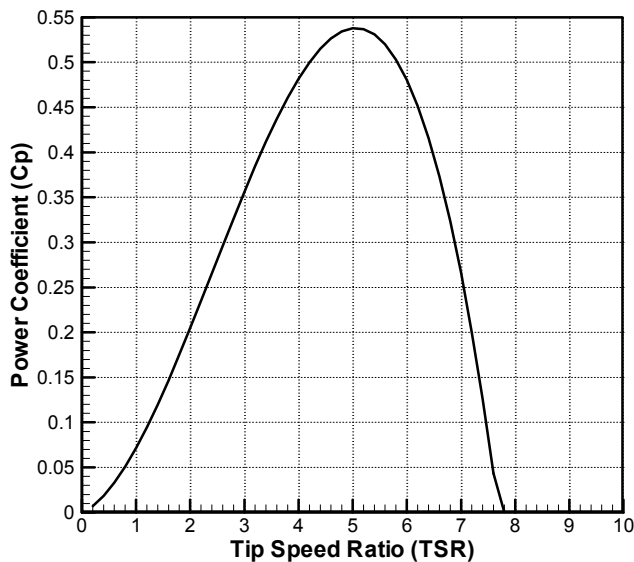


Figure 13. Power coefficient with tip speed ratio.

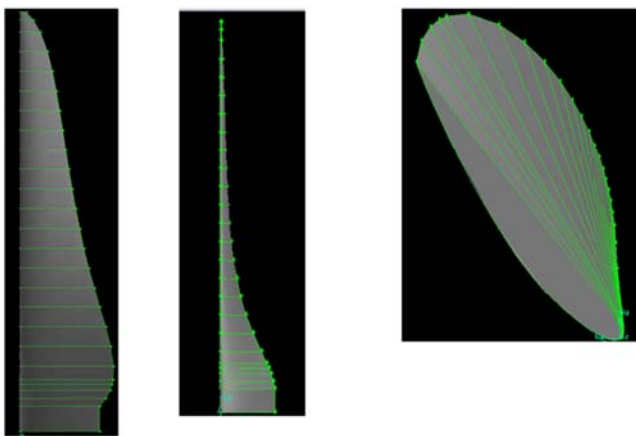


Figure 14. Three-dimensional views of wind turbine blade.

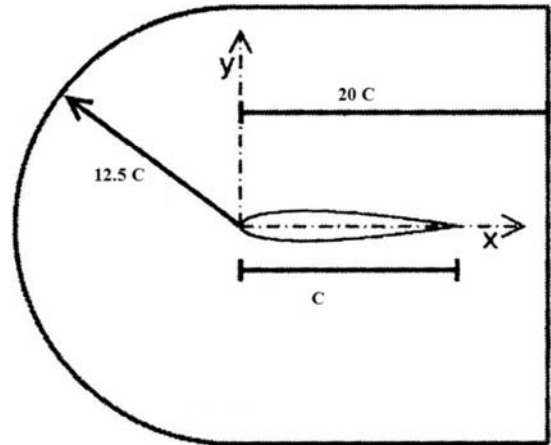


Figure 15. Computational domain of NACA 4412 airfoil. (Not to Scale).

To generate grid – independency of the solution, computations were carried out for a wide range of the grid size (from 90,000 to 500,000 cells) at blade angle. The judging parameters were the lift and drag coefficients.

From figure (16), it is clear that there is no change of the values of the lift and drag coefficients after the grid size of 450,000 cells.

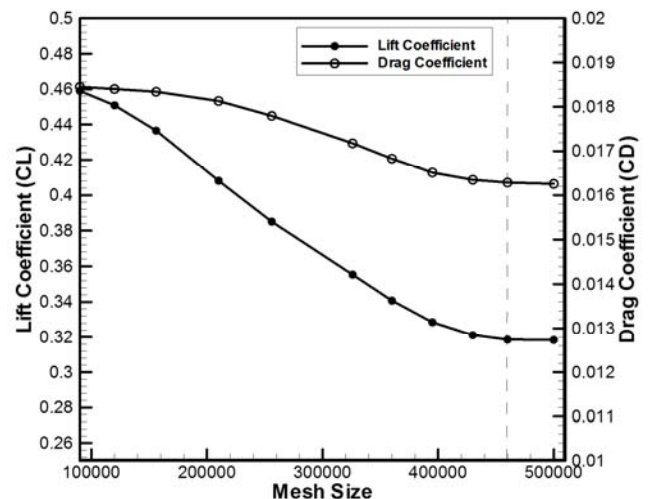


Figure 16. Mesh Sensitivity.

Thus, the grid consisted of 450,000 quadrilateral cells. A large number of grid cells was concentrated around the aerofoil surface to capture the pressure gradient accurately in the boundary layer. This is because the adverse pressure gradient induces flow separation. Stall occurs when separation region extends. In the far-field region, the mesh resolution becomes progressively coarser since the flow gradients approach zero. The meshing overview is shown in Figure (17).

Pressure far-field boundary condition was used in the computational domain which is large enough. Aerofoil was treated as stationary-wall boundary condition with no slip shear condition. Unsteady simulations were carried out with viscosity $1.7894 \times 10^{-5} \text{ kg/m.s}$, air density, and wind speed 6 m/s . Shear-stress transport (SST) $k-\omega$ model was used

because it absorbs both the property of good accuracy in the near-wall region of standard $K - \omega$ model and nice precision in the far field region of $K - \omega$ model [6].

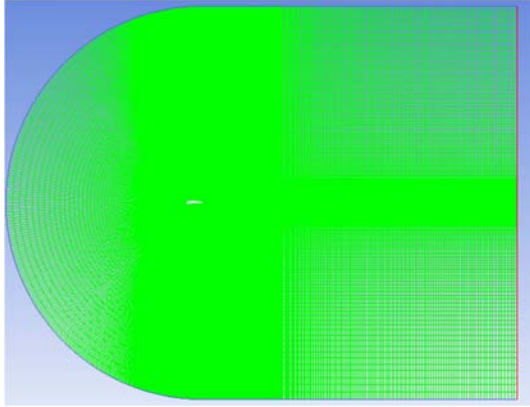


Figure 17. NACA 4412 meshing using structured grid.

5.2. Computational Results and Discussions

Figures (18) – (27) show the vorticity, velocity, and pressure coefficient contours for the profile of the wind turbine blade at different blade angles compared with velocity contours of [3].

Figure (18) shows the vorticity, velocity, and pressure coefficient contours for the airfoil profile of the wind turbine blade at zero blade angle. The vortex generated behind the airfoil is very thin due to zero blade angle. As expected, pressure on the upper surface is less than the pressure on the lower surface but velocity on the upper surface is higher than the velocity on the lower surface of the airfoil. Figure (18d)

shows the counters of velocity at zero blade angle for NACA 4420 airfoil [3]. Comparing figure (18b) with figure (18d), the change of velocity has the same trend and results of NACA 4412 are really acceptable in comparison to the result of NACA 4420 [3].

Figure (19) shows the vorticity, velocity, and pressure coefficient contours for the airfoil profile of the wind turbine blade at 10° blade angle. The vortex that appears behind the airfoil is bigger than that of zero blade angle. The change of pressure and velocity around the airfoil is more than that of zero blade angle.

Figure (20) shows the vorticity, velocity, and pressure coefficient contours for the airfoil profile of the wind turbine blade at 20° blade angle. The vortex generated behind the airfoil covers a large area. Figure (20d) shows the counters of velocity at 22.5° blade angle for NACA 4420 airfoil [3]. Comparing figure (20b) with figure (19d) the distribution of velocity has the same trend and results of NACA 4412 are generally acceptable in comparison to the results of NACA 4420 [3].

Figure (21) – (27) show the vorticity, velocity, and pressure coefficient contours for the airfoil profile of the wind turbine blade at different blade angles. The vortex generated behind the airfoil is covers a larger area as the blade angle increases. By increasing the blade angle, the change of pressure and velocity around airfoil increases. Comparing the results with the results of NACA 4420 airfoil [3], the change of velocity has the same trend and results of NACA 4412 are acceptable in comparison of the result of NACA 4420 [3].

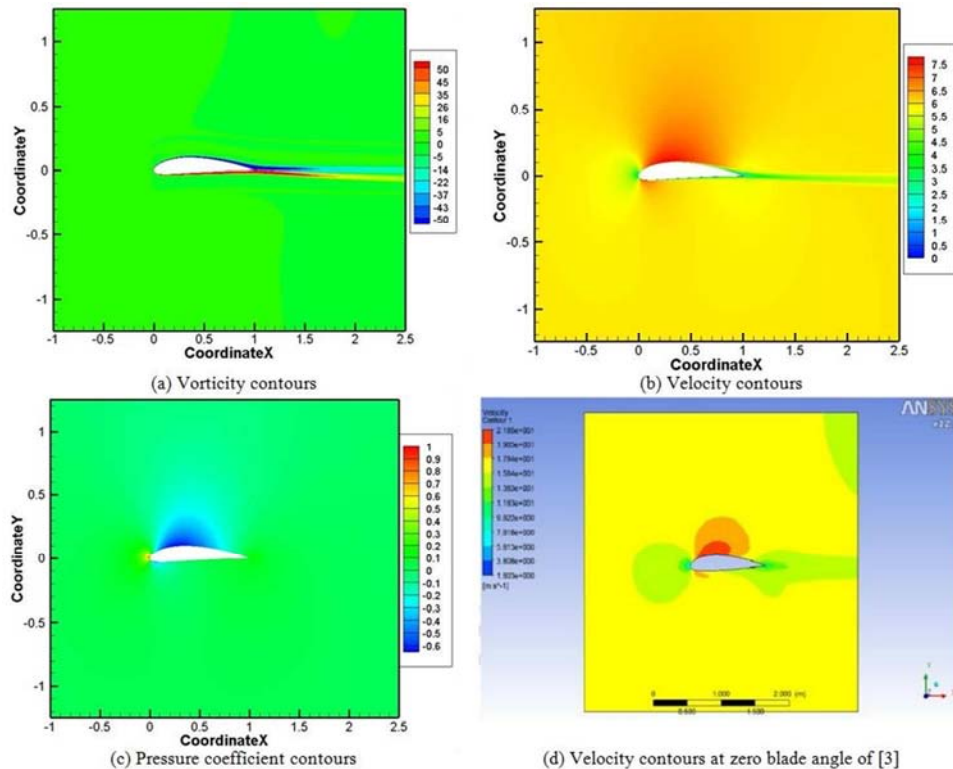


Figure 18. Blade Angle = 0° .

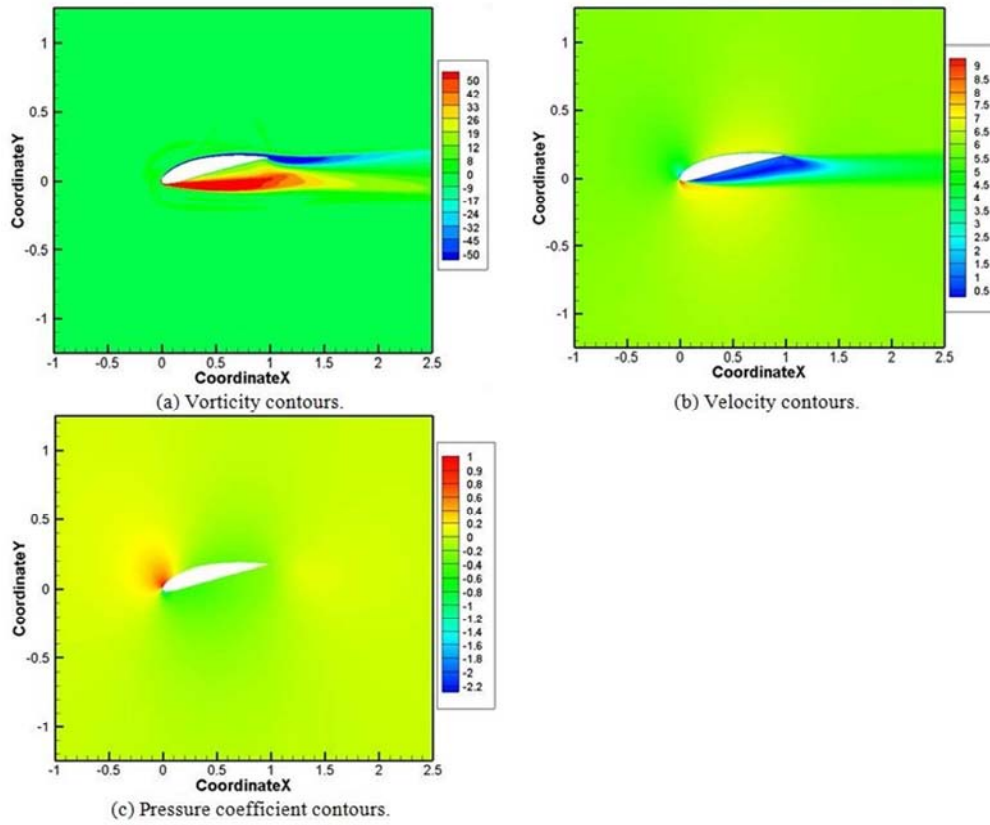


Figure 19. Blade Angle = 10^0 .

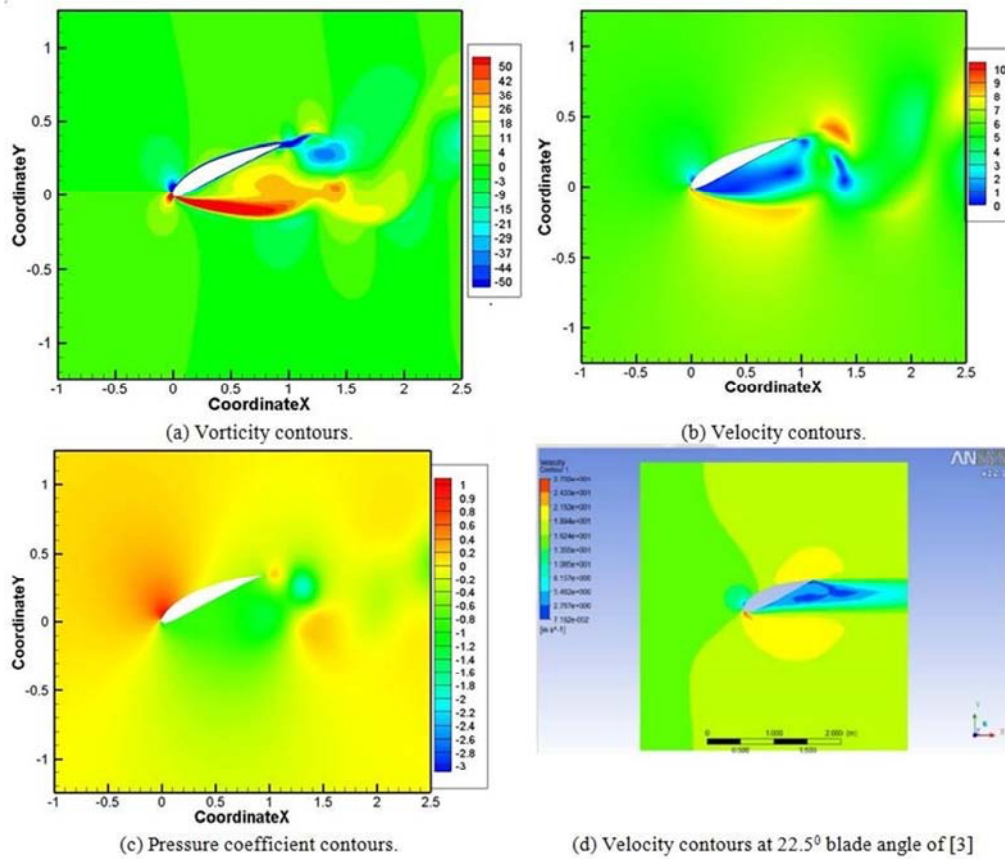
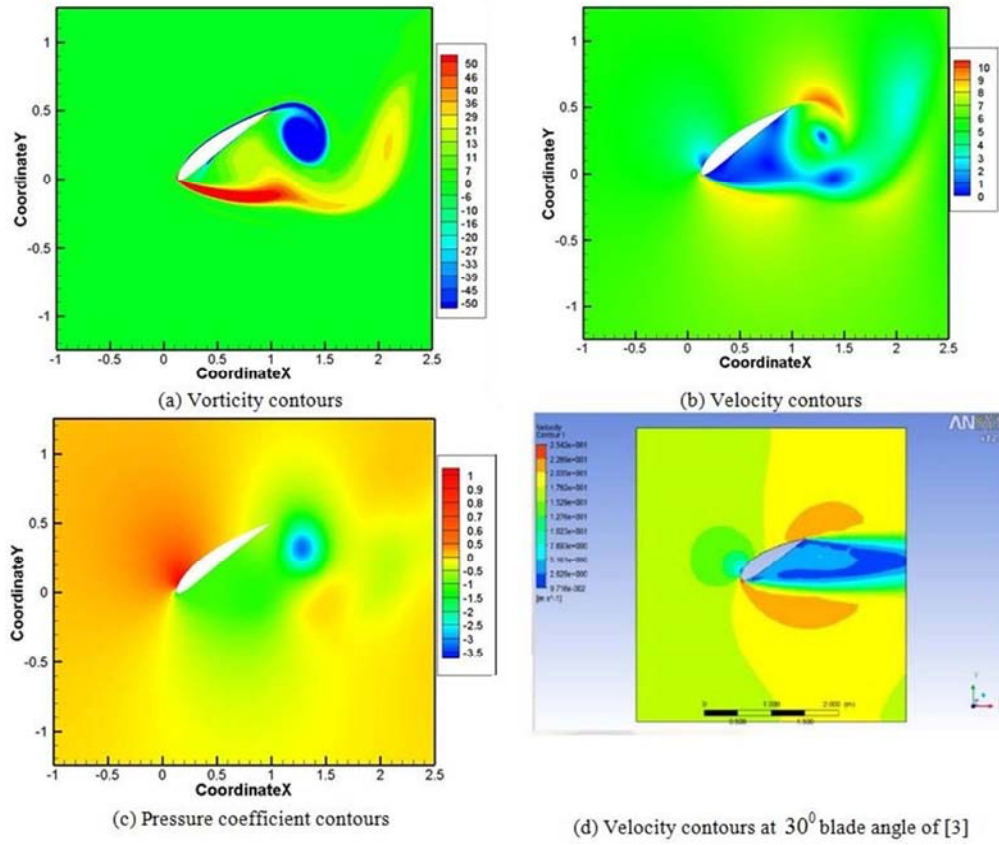
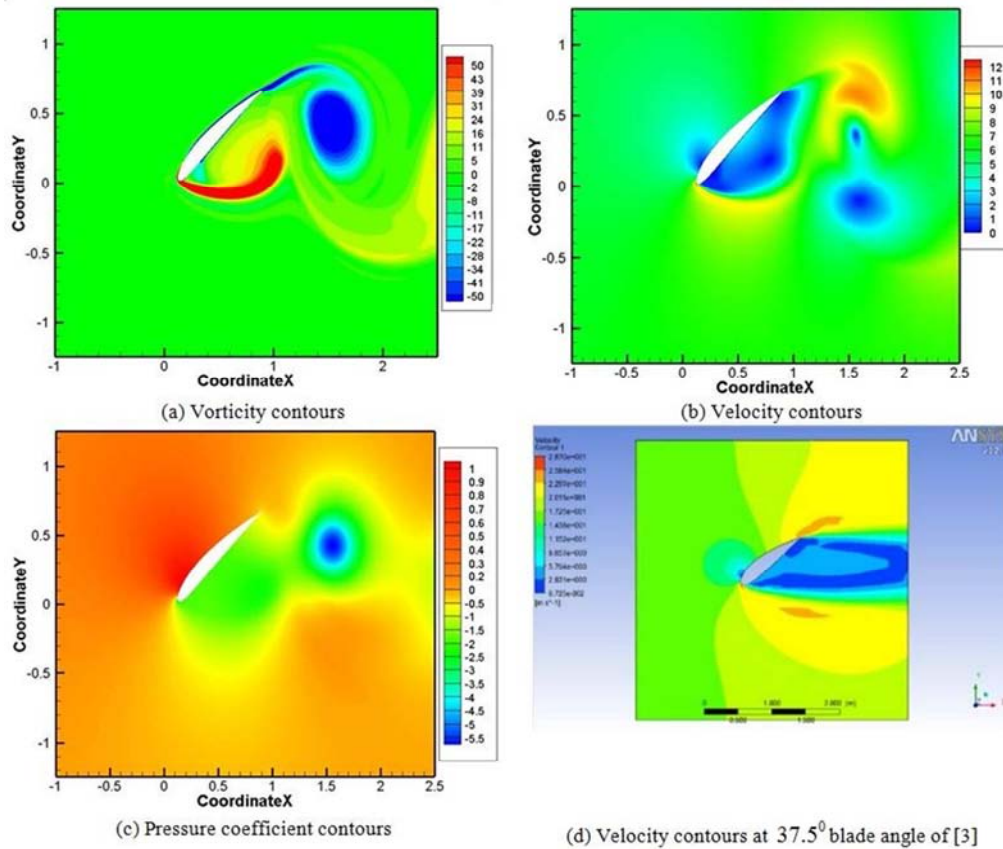
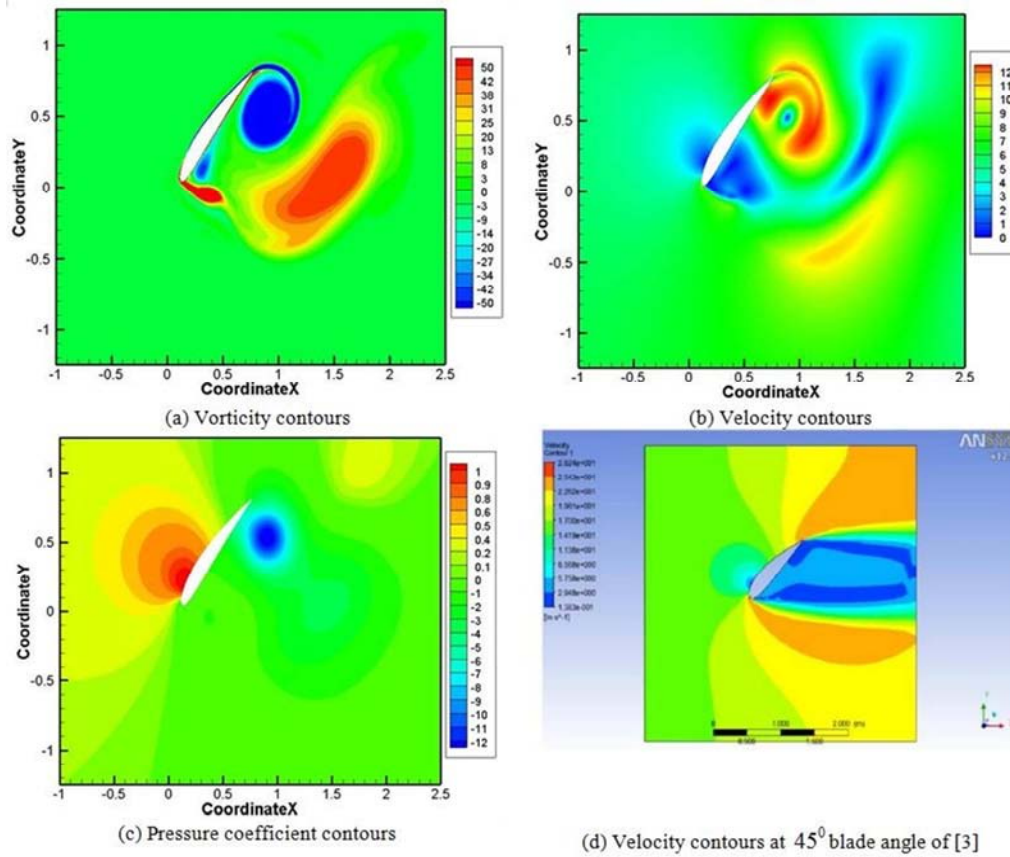
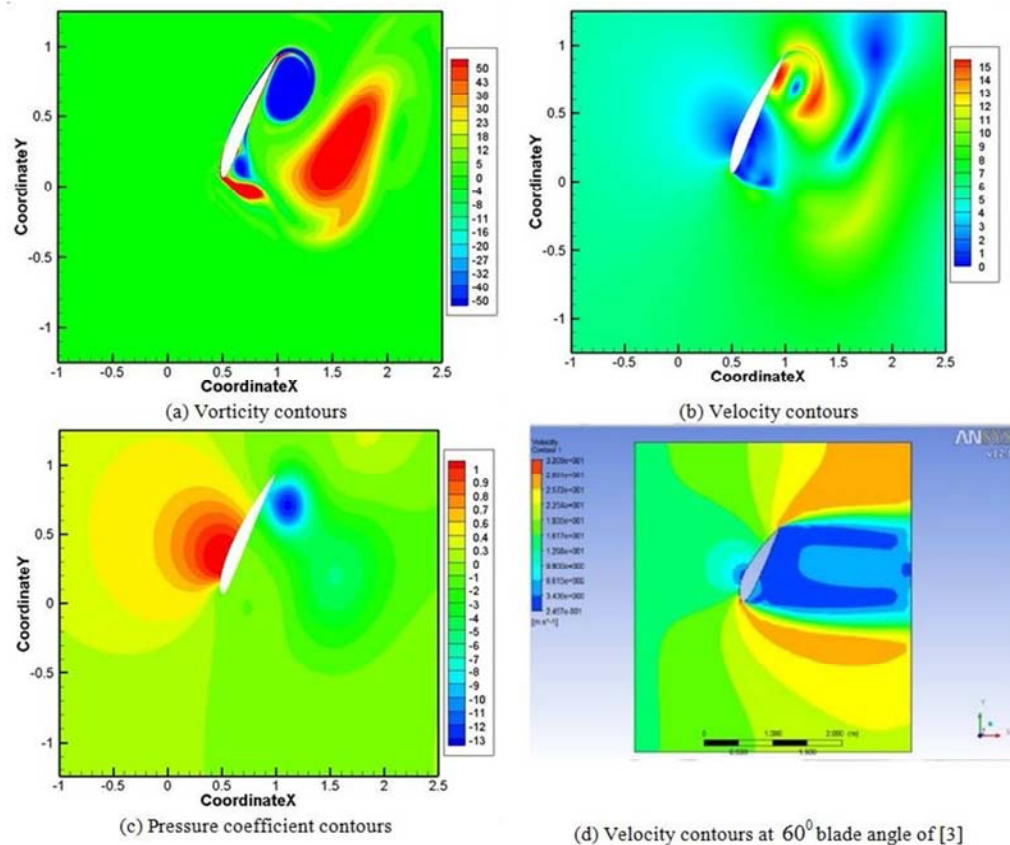


Figure 20. Blade Angle = 20^0 .

Figure 21. Blade Angle = 30° .Figure 22. Blade Angle = 40° .

Figure 23. Blade Angle = 50° .Figure 24. Blade Angle = 60° .

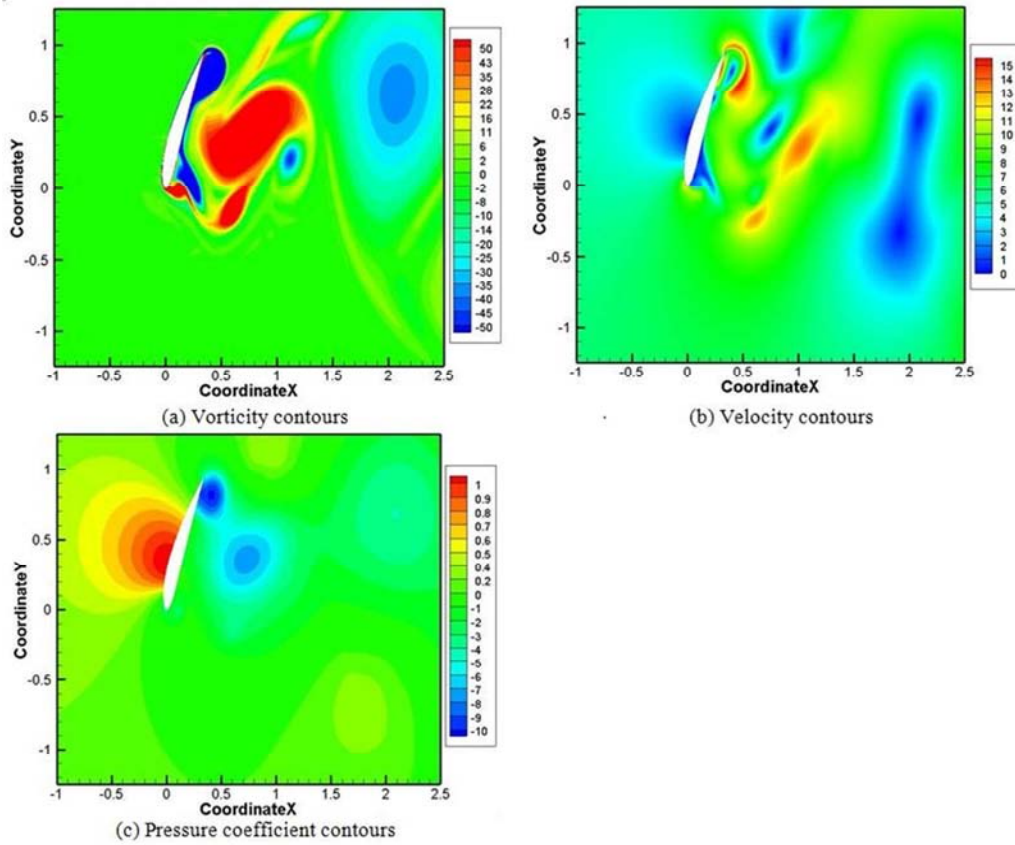


Figure 25. Blade Angle = 70° .

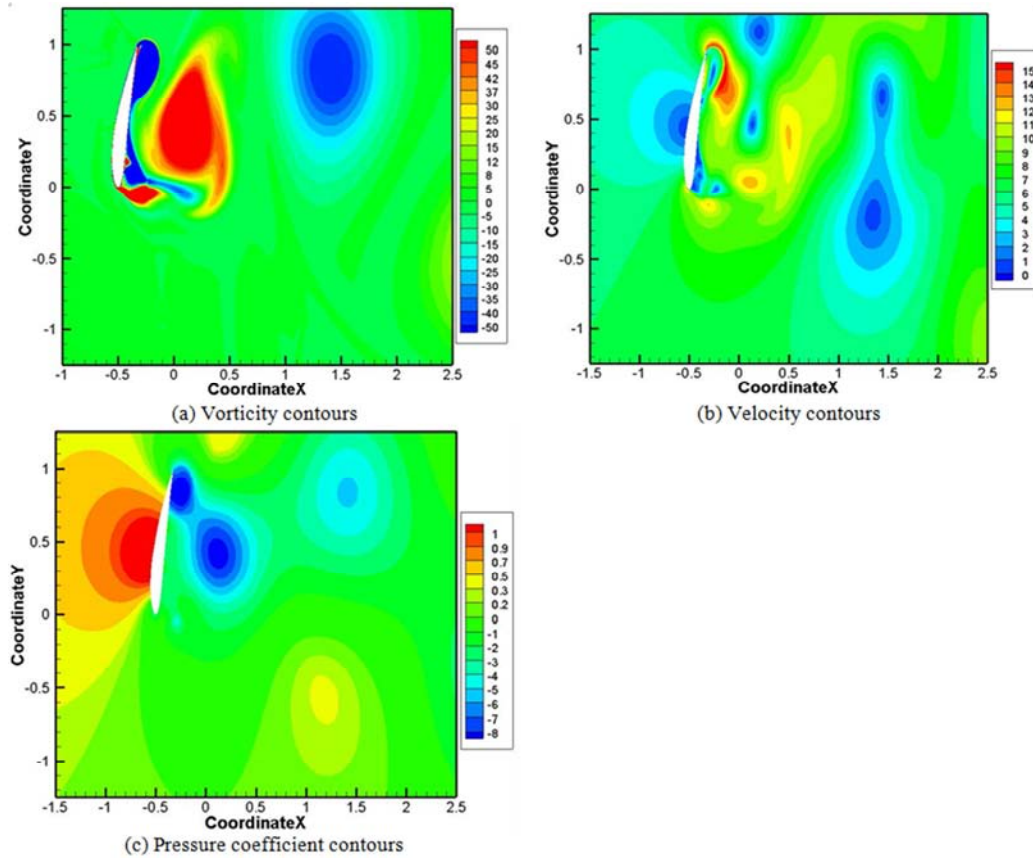


Figure 26. Blade Angle = 80° .

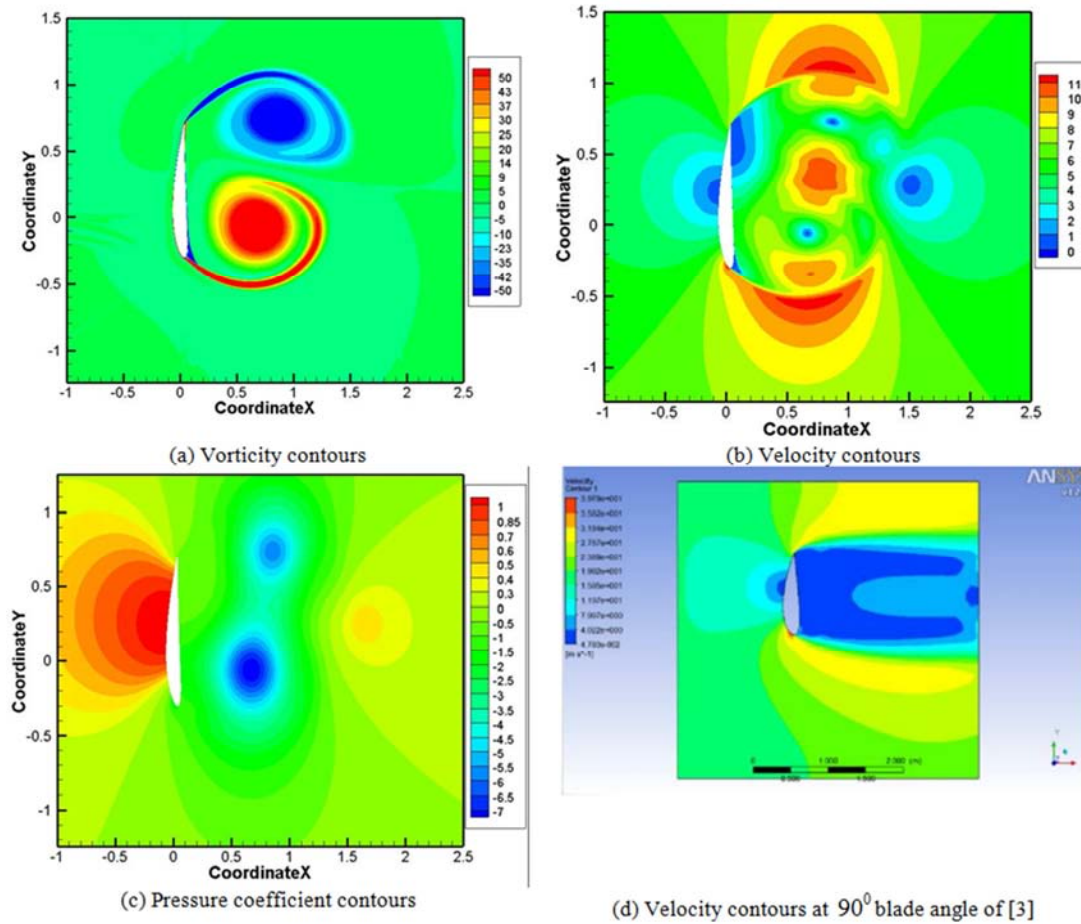


Figure 27. Blade Angle = 90° .

From Figures (18) – (27), velocities are obtained for different blade angles. Power produced from the wind is given by the following:

(1) Wind power can be calculated from the following equation:

$$P_w = \frac{1}{2} \rho V^3 A \quad (16)$$

where: P_w = power produced from the wind

ρ = air density is taken as 1.225 kg/m^3

A = wind turbine projected area =

$$\pi [R_t^2 - R_h^2] = \pi [(0.35)^2 - (0.035)^2] = 0.381 \text{ m}^2$$

V_w = wind speed is taken as 6 m/s .

(2) Maximum generated power may be obtained from the wind turbine can be calculated from the following equation:

$$P_{\max} = \frac{1}{2} \rho V^3 A \times \frac{16}{27} \quad (17)$$

Table (3) was obtained from the calculations of wind power and maximum generated power may be obtained from the turbine with respect to velocity.

Table 3. Wind power and maximum power for different blade angle.

Blade Angle	Velocity (V)	Wind Power (P_w)	Maximum Generated Power
0	5.835	46.360	27.473
10	5.910	48.172	28.546
20	6.000	50.406	29.870
30	6.025	51.039	30.245
40	6.045	51.549	30.548
50	6.053	51.754	30.669
60	6.10	52.969	31.389
70	6.31	58.630	34.744
80	6.43	62.039	36.764
90	6.70	70.187	41.592

Figure (28) shows the change of air velocity impact the blade at different blade angles. It is clear that the air velocity increases with the increase in blade angle from (5.835 m/s) at (0°) to (6.7 m/s) at (90°). From angle (20°) to (60°), the increase in velocity is small; from (6 m/s) to (6.1 m/s), then, air velocity increases sharply with the increase of the blade angle. The air velocity reaches the maximum value when blade angle equals to (90°).

Figure (29) shows the change of wind power at different blade angles. It is clear that the wind power increases with the increase in blade angle from (46.36 W) at (0°) to (70.187 W) at (90°). From angle (20°) to (60°), the increase in wind power is small; from (50.406 W) to (52.969 W), then, wind power is increases sharply with the increase of the blade angle. The wind power reaches the maximum value when blade angle equal to (90°).

Figure (30) shows the maximum power that may be generated by the turbine [3] which has the hub diameter of 0.3375 m, blade length of 10.7 m, NACA 4420 airfoil profile and wind speed of 16 m/s .

Comparing Figure (29) and (30), the present study gives the power at different angles which increases with the increase of blade angle. For blade angle change from 20° to 60° , the wind power has a small increase and reaches the maximum when blade angle equals to 90° . This change of power with the blade angle is near from that of other published data [3].

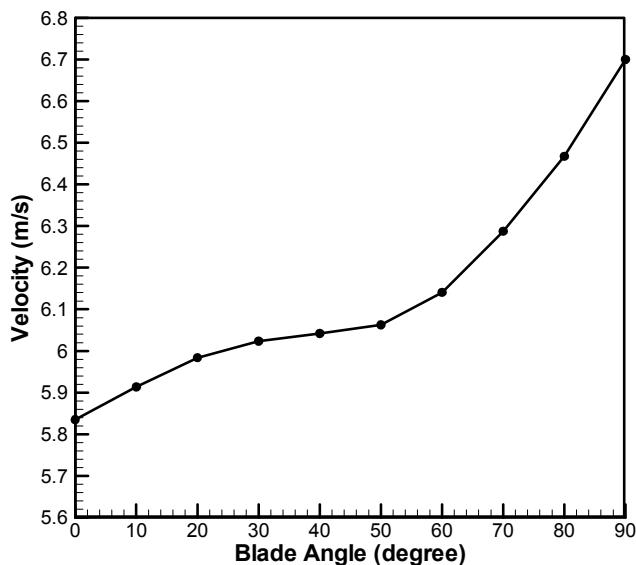


Figure 28. Air velocity impact the blade at different blade angles.

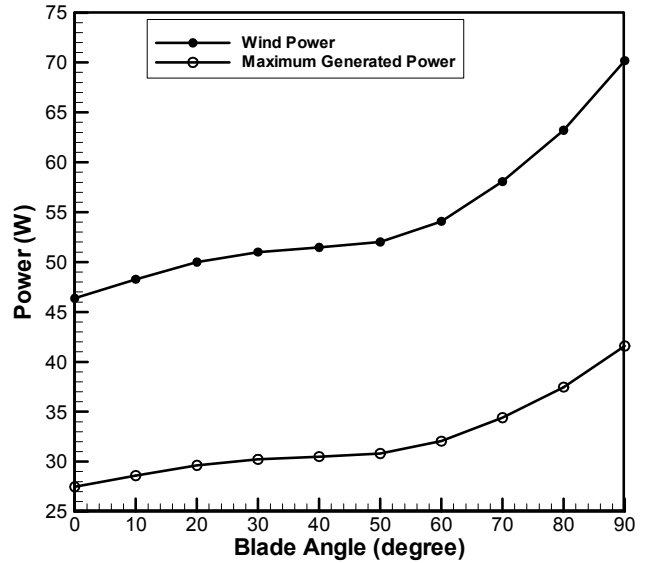


Figure 29. Power at different blade angles.

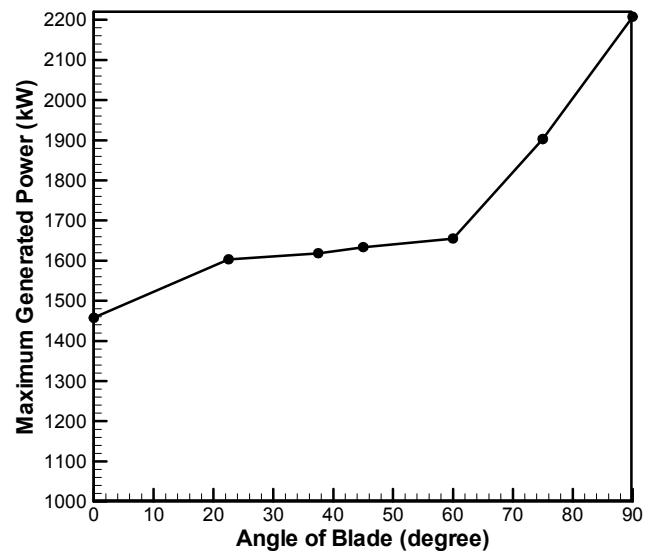


Figure 30. Maximum power that may be generated from wind turbine of [3].

6. Conclusions

In this paper, a horizontal–axis wind turbine blade with NACA 4412 profile was designed and analyzed for different blade angles and wind speeds. CFD analysis was carried out using ANSYS Fluent software. The vorticity, velocity and pressure distributions at various blade angles were discussed. The present results are coinciding with the published data of others. From results, it is seen that the wind power is increased by increasing the blade angle due to the increase in air velocity impacting the wind turbine blade. For blade angle change from 20° to 60° , the wind power has a small increase and reaches the maximum when blade angle equals to 90° . Thus, HAWT output power depends on the blade profile and its orientation.

Nomenclature

A	Area of wind turbine rotor	Q	Rotor torque
a	Axial induction factor at rotor plane	R_{tip}	Tip radius of wind turbine rotor
a'	Angular induction factor	$r(i)$	Local radius of any point on the blade
B	Number of blades of a rotor	T	Rotor thrust
C	Blade chord length	U	Freestream velocity of wind
C_D	Drag coefficient of an airfoil	α	Angle of attack
$C(i)$	Blade chord length for the i^{th} blade element	α_{design}	Design angle of attack
C_L	Lift coefficient of an airfoil	ϕ	Angle of relative wind velocity with rotor plane
$C_{L,design}$	Design lift coefficient of an airfoil	λ	Tip-speed ratio of rotor
C_P	Power coefficient of wind turbine rotor	$\lambda_{r,i}$	Local tip-speed ratio for the i^{th} blade element
$C_{P,max}$	Maximum rotor power coefficient	ρ	Air density
F	Tip-loss factor	σ	Solidity ratio
$F(i)$	Tip-loss factor for the i^{th} blade element	θ	Blade setting angle (blade twist angle)
N	Number of blade elements	Ω	Angular velocity of wind turbine rotor
P	Power output from wind turbine rotor		

References

- [1] Burton, T., and Sharpe, D., "Wind Energy Handbook", John Wiley & Sons Ltd, Chichester, 2006.
- [2] Cao H., "Aerodynamics Analysis of Small Horizontal Axis Wind Turbine Blades by Using 2D and 3D CFD Modelling", University of Central Lancashire, Preston, England, MSc. Thesis, 2011,
- [3] Chandrala A., "Aerodynamic Analysis of Horizontal Axis Wind Turbine Blade", International Journal of Engineering Research and Applications (IJERA), Vol. 2, Issue 6, November- December 2012, pp.1244-1248.
- [4] Chaudhary M., and Roy A., "Design & Optimization of a Small Wind Turbine Blade for Operation at Low Wind Speed", International Journal on Recent Technologies in Mechanical and Electrical Engineering (IJRMEE), ISSN: 2349-7947, Vol. 2, Issue: 3, March 2015.
- [5] Derakhshan S., and Tavaziani A., " Study of Wind Turbine Aerodynamic Performance Using Numerical Methods", Journal of Clean Energy Technologies, Vol. 3, No. 2, March 2015
- [6] Fluent, ANSYS FLUENT 12.0 Theory Guide, ANSYS Inc., April 2009.
- [7] [Http://en.wikipedia.org/wiki/Smock_mill](http://en.wikipedia.org/wiki/Smock_mill)
- [8] [Http://guidedtour.windpower.org/en/core.htm](http://guidedtour.windpower.org/en/core.htm)
- [9] Hu H., Li X., and Gu B., "Flow Characteristics Study of Wind Turbine Blade with Vortex Generators", International Journal of Aerospace Engineering Vol. 2016, Article ID 6531694, 11 pages.
- [10] Kale S., and Sapali S., "Functional and Strength Design of one MW Wind Turbine Blade", proceedings of international conference on energy and environment, March 19-21, 2009 ISSN: 2070-3740.
- [11] Kulunk E., and Yilmaz N., "Computer – Aided Design and Performance Analysis of HAWT Blades" 5th International Advanced Technologies Symposium (IATS'09), May 13-15, 2009, Karabuk, Turkey.
- [12] Kumar V. M., Rao B. N., and Farooq S., "Modeling and Analysis of Wind Turbine Blade with Advanced Materials by Simulation", International Journal of Applied Engineering Research, ISSN 0973-4562, Vol. 11, No 6, (2016), pp. 4491-4499.
- [13] Marten D., and Wendler J., "QBlade Guidelines v0.6", 2013.
- [14] Manwell J., McGowan, J., and Rogers, A., "Wind Energy Explained. Theory, Design and Application", 2nd edn., John Wiley and Sons Ltd., ISBN 978 0 470 015001, 2009.
- [15] Mostafa R., Ali A., and Nassr A., " Power Regulation for Variable Speed Variable Pitch HAWT Pitch and Torque Control Strategy", Research Journal of Applied Sciences, Engineering and Technology, Vol. 12, No. 3, pp. 366-374, 2016.
- [16] Tenguria1 N., Mittal1 N., and Ahmed S., "Structural Analysis of 38.95 m Horizontal Axis Wind Turbine Blades", International Journal of Mechanical and Materials Engineering (IJMME), Vol.6, No.2, pp. 183-188, 2011.
- [17] Wood D., "Small Wind Turbines Analysis, Design, and Application", Springer-Verlag London Limited, 2011.